Available online at www.sciencedirect.com
SCIENCE DIRECT®
Journal of Crystal Growth 269 (2004) 111–118
JOURNAL OF CRYSTAL GROWTH
www.elsevier.com/locate/jcrysgro

The influence of structural properties on conductivity and luminescence of MBE grown InN

P. Specht[a,b,*], R. Armitage[a], J. Ho[a,b], E. Gunawan[b], Q. Yang[a,b], X. Xu[a,c], C. Kisielowski[c], E.R. Weber[a,b]

[a] *Lawrence Berkeley National Laboratory, Materials Science Division, University of California, Berkeley, CA 94720, USA*
[b] *Department of Materials Science and Engineering, University of California, Berkeley, CA 94720, USA*
[c] *National Center of Electron Microscopy, Lawrence Berkeley National Laboratory, One Cyclotron Road, Berkeley, CA 94720, USA*

Abstract

Within the last few years indium nitride (InN) gained substantial interest due to its controversially discussed apparent band gap and its predicted highest maximum electron mobility among several III–V compounds, including Al(Ga)N and GaAs. The band gap of epitaxial InN has been recently reported to be around 0.7 eV rather than the previously accepted value of 1.9 eV obtained from polycrystalline films. Thus, InN could be a promising material for applications in infrared opto-electronics or high-speed electronics. However, the structural quality of the InN epilayers is still inferior to GaN and needs to be improved. Also, the role of many contaminants in InN and their effect on the epilayer's conductivity and/or luminescence properties is still under investigation.

This work describes recent studies of InN growth by molecular beam epitaxy on sapphire (0 0 0 1) substrates. The effect of buffer layer variations including a prior substrate nitridation step is discussed. Structural properties (X-ray diffraction, AFM and TEM images) and chemical profiles (SIMS) will be correlated to Hall data and Photoluminescence spectra. The role of oxygen and hydrogen as possible donors in InN will be discussed.

PACS: 81.15.H; 61.10.N; 68.55.L

Keywords: A1. Crystal structure; A1. Impurities in thin films; A1. X-ray diffraction; A3. Molecular beam epitaxy; B1. Indium nitride

1. Introduction

The fundamental knowledge of indium nitride (InN) is still very limited at present. Even basic properties such as its electronic band gap are debated controversely. The deposition of InN epilayers requires low-temperature growth due to the highest equilibrium nitrogen partial pressure per relative growth temperature ($T_{\text{growth}}/T_{\text{melting}}$) among the group III-nitrides [1]. However, the material also exhibits the highest reported peak electron drift mobility [1] while simultaneously providing an exceptionally high free electron concentration. Recently, InN epilayers

*Corresponding author. Lawrence Berkeley National Laboratory, Materials Science Division, University of California, Bldg. 62-113, One Cyclotron Road, Berkeley, CA 94720, USA. Tel.: +1-510-495-2934; fax: +1-510-486-4995.
E-mail address: specht@socrates.berkeley.edu (P. Specht).

0022-0248/$ - see front matter © 2004 Published by Elsevier B.V.
doi:10.1016/j.jcrysgro.2004.05.097

have reproducibly been grown with electron mobility values exceeding 1000 $cm^2/V\,s$ [2]. Consequently, the initially most prominent application concentrated on ultrafast transistor technology. The fundamental bandgap of InN was generally accepted to be around 1.9 eV [3,4]. Very recently, researchers in Russia and the USA suggested it to be close to 0.7 eV [5,6]. The latter group suggested that in samples with high electron concentration the Moss–Burstein effect shifts the fundamental band gap towards higher energies. This discovery started an effort to develop InN for solar cell technology and other opto-electronic applications. A low InN bandgap would complete the coverage of the solar energy spectrum by detectors built from the (In,Ga,Al)N alloy system, thereby providing highest efficiency multi-junction solar cell materials or all-color III-nitride general lighting (for example see Ref. [7]).

While the highest contaminated InN epilayers discussed in this paper contain up to one percent of oxygen recent investigations of molecular beam epitaxy (MBE) grown InN epilayers report three to four orders of magnitude lower oxygen concentration [8]. Oxygen can act as a donor in all group III-nitrides and consequently, oxygen contamination was often assumed to be responsible for the high unintentional n-type doping in MBE grown InN. The lattice constants of the wurtzite InN crystal are the largest of the group III-nitrides and to date no lattice-matched substrate is available for InN epilayer growth. Growth on a largely mismatched substrate generates large strain. Fig. 1 shows how stresses translate into strains for GaN, AlN and InN single crystals. The maximal stress values used for the strain calculation in Fig. 1 are ± 1.2 GPa, elastic constants were taken from Wright [9]. Shown are strains that result from hydrostatic stresses (triangles), biaxial stresses along the basal planes (stars) and linear stresses along the c-axis (circles) of the respective GaN, AlN or InN crystals. Hydrostatic stresses may result from the homogeneous incorporation of point defects. Biaxial stresses are often the result of a lattice mismatch to the substrate and linear stresses in c lattice direction are known to occur if point defects are incorporated preferentially along the basal planes. Fig. 1 shows that InN crystals

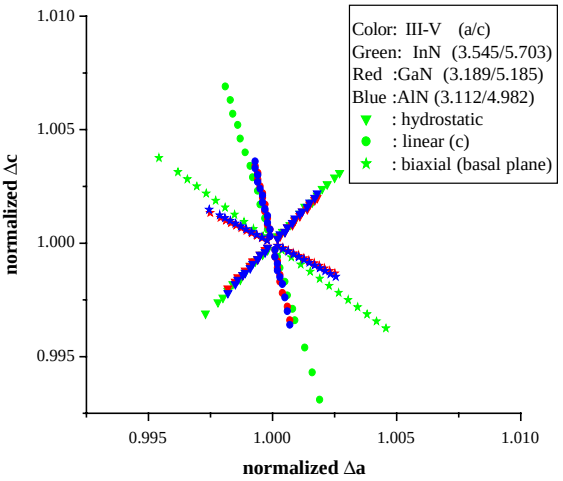

Fig. 1. Anisotropic stress response in III-nitrides, in normalized lattice constants c/c_0 versus a/a_0. Compared are GaN (red), AlN (blue) and InN (green), elastic constants taken from Ref. [15].

will have to sustain larger crystal deformations than GaN or AlN crystals at similar stress levels. One also needs to take into account that InN crystals are grown at an even lower relative growth temperature than the other group III-nitride compounds. LT-growth can result in higher concentrations of native defects and/or contaminants in the crystals [10] which add to the epilayer strain. It is therefore quite remarkable that InN epilayers can be grown at all with decent crystalline quality. This study is focused on an analysis of structural properties of MBE grown InN epilayers, their dependence on the growth parameters and their impact on opto-electronic properties.

2. Experimental procedure

InN epilayers were grown by MBE in a Riber 1000 system. A standard In effusion cell and a DC nitrogen plasma source were used. The layers were deposited on (0 0 0 1) sapphire substrates at growth temperatures around 500°C (pyrometer readings, assumed emissivity: 0.9) and under In-rich conditions. Common growth rates are about 0.2 μm/h, and the InN film thickness is around 1 μm. Prior to the epitaxial growth a nitridation step was

Table 1
InN epilayer properties and buffer layer identification

Sample No.	Buffer layer	average [O] (cm^{-3})	[n]: Hall (cm^{-3})	Mobility ($cm^2/V\,s$)	FWHM (0 0 0 2) (arcmin)
901	MBE GaN	4×10^{20}	5×10^{20}	50	14
902	MBE GaN	$>10^{20}$	3.3×10^{20}	59	8
903	MBE GaN	$>10^{20}$	1.9×10^{20}	160	—
904	MOVPE GaN	$>10^{20}$	3.4×10^{20}	43	11
905	MOVPE GaN	$>10^{20}$	3.5×10^{20}	88	10
910	AlN	$>10^{20}$	1.4×10^{20}	134	8
920	AlN	1×10^{20}	1.8×10^{20}	155	6
J5	AlN	Not avail.	3.7×10^{19}	447	6
J6	AlN	Not avail.	9.7×10^{19}	263	6
J7	AlN	1×10^{19}	7.8×10^{19}	360	5
J8	AlN	$>10^{19}$	7.2×10^{19}	515	6
J10	AlN	2×10^{19}	2.8×10^{19}	67	5
J19	AlN	2×10^{19}	8.2×10^{18}	28	11
J21	AlN	1×10^{18}	5.5×10^{19}	280	5

introduced which resulted in the formation of a thin AlN buffer layer. Two sets of epilayers were grown, set I: #901-#920, contains approximately one order of magnitude higher oxygen concentration than the set II: J3-J21, as will be shown below. Also, for some of the layers in the first set a GaN buffer layer was used along with a nitrided sapphire substrate. In those cases the different buffer layers will be mentioned in the following text. Different buffer layers are also marked in Table 1.

3. Results and discussion

Fig. 2 shows a cross-sectional TEM micrograph of an epilayer structure of set I. The InN epilayer was deposited on an approx. Thirty nanometer thick MBE grown GaN buffer layer. The InN film exhibits the typical high dislocation density of a highly mismatched, relaxed hetero-epitaxial structure. The GaN buffer layer can be identified in both images, either through clearly visible interfaces (overview) or through energy-filtered (EF)-TEM revealing indium or nitrogen.

AFM images show that the different sets of samples exhibit distinctly different surface morphology (Fig. 3). While the surfaces of set I samples are dominated by small triangular shapes, the film surfaces of set II samples are smoother and contain on average grains with larger dimensions than those of set I. Similar surface morphology to those of set II samples have also been observed for In-polar InN epilayers by Xu and Yoshikawa [11]. In the TEM image, Fig. 2, the typical-triangular shaped surface features of set I films are also visible. For most epilayers, elongated grains were found with a width around 10% of their respective lengths. Exceptionally, small grain sizes were observed in sample J19 (set II) with approx. 300 nm length. One thousand nanometer long grains were obtained in samples #904 and #905 (set I). J19 was deposited with intentionally high background pressure in an (unsuccessful) effort to reproduce high concentrations of oxygen incorporation. This resulted in a partial compensation of the dominant donors. Samples #904 and #905 were deposited on MOVPE GaN buffer layers. However, even those samples show characteristic surface features which is interpreted to be a result of the difference in oxygen concentration.

High-resolution X-ray diffraction spectra of the symmetric (0 0 h) reflexes, $h=2,4,6$, and asymmetric (1 0 1), (1 0 2), (2 0 2) and (2 0 4) reflexes were taken in a normal coupled scan mode. Interplanar distances were calculated as described in Ref. [12] for wurtzite GaN epilayers. From those values the a and c lattice constants were determined. Fig. 4 summarizes the lattice constants obtained in this way for both sample sets,

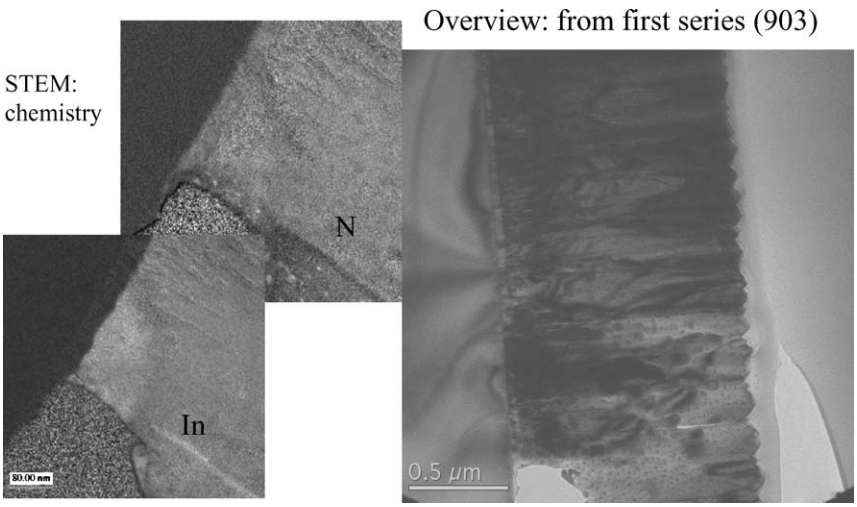

Fig. 2. TEM micrograph of an InN epilayer (#903) grown on (0 0 0 1) sapphire with an MBE grown 30 nm thick GaN buffer layer. Left images: energy-filtered TEM of nitrogen and indium, right image: TEM micrograph with typical columnar growth of InN.

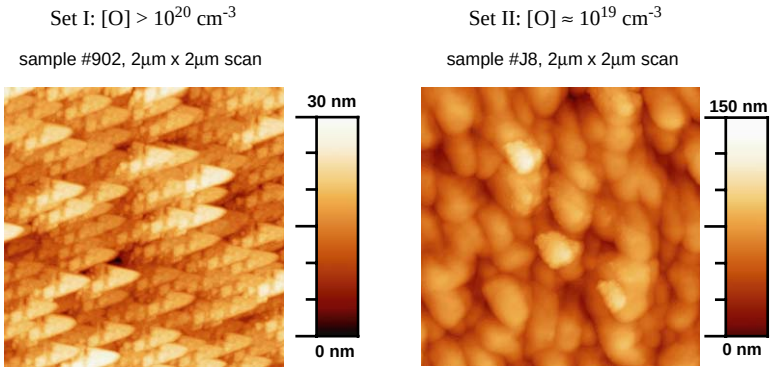

Fig. 3. AFM surface images of set I (left) and set II (right) InN epilayer.

including the calculated (pure) strain types for InN (from Fig. 1). For comparison literature results are included of a bulk crystal from Paszkowicz, et al. [13]. The first growth series (full squares in Fig. 4) exhibits a larger variation of lattice constants than the second series because of more changes in growth conditions and the large incorporation of oxygen (up to 1%, see Table 1) and other point defects. Most epilayers of set II vary only slightly from the bulk crystal value. The residual difference in lattice parameter is likely related to specific growth conditions of some epilayers rather than to their specific contamination content. Samples J5 and J6 were exposed to a prior substrate nitridation process at a lower temperature than all other samples of this series (set II). J5 has the highest variation of lattice constants and the lowest substrate temperature during nitridation. Growth of sample #904 was already described earlier, the epilayer exhibits a very high linear stress response (approx. 3 GPa). J19 exhibits a lattice constant close to the strain-free value [9] despite a high concentration of contaminants present in the epilayer.

SIMS profiles were obtained from selected samples of both series. The oxygen and hydrogen

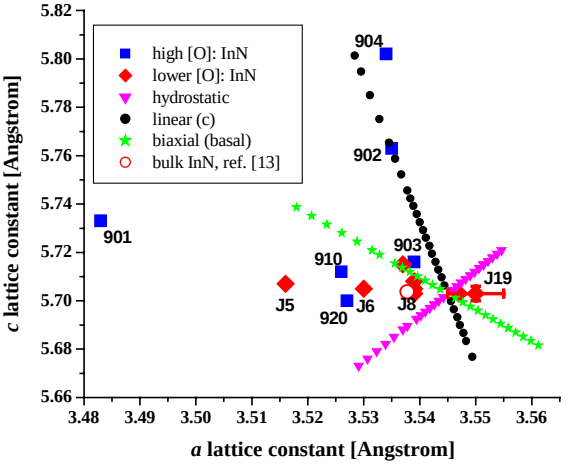

Fig. 4. Lattice constants determined by high-resolution X-ray diffraction of various InN crystals. The literature values of a bulk crystal [13] are given for comparison. Also shown are the theoretical lattice constant changes for an InN crystal under pure uni-axial (*c*-direction), biaxial (basal plane) and hydrostatic stress.

concentrations were calibrated [8], all other SIMS signals are in quasi-arbitrary units, that is, their intensity was first approximated using GaN standards, then adjusted proportionally to the calibrated oxygen and hydrogen concentrations. The calibration of SIMS profiles of other chemical elements (e.g. Si, S, C, Mg) in InN is in progress. Fig. 5a and b gives two examples of SIMS profiles from the second sample series. The InN profile provides the location of the epilayer. The average oxygen concentration remains in the low $10^{19}\,cm^{-3}$ range which is typical for set II samples. In samples grown after J19 the oxygen concentration was found to be reduced by one order of magnitude (low $10^{18}\,cm^{-3}$ range). The hydrogen concentration increased by a factor of 4 in J19 ($8\times10^{18}\,cm^{-3}$) while the carbon, silicon and sulphur concentrations remained approximately constant (no absolute value, see above). The average oxygen concentration of selected samples is given in Table 1.

The free electron concentration and electron mobility of the InN epilayers were measured in Van-der-Pauw geometry. Maximum mobility was measured for set I epilayers around $150\,cm^2/V\,s$ and for set II epilayers around $500\,cm^2/V\,s$. Table

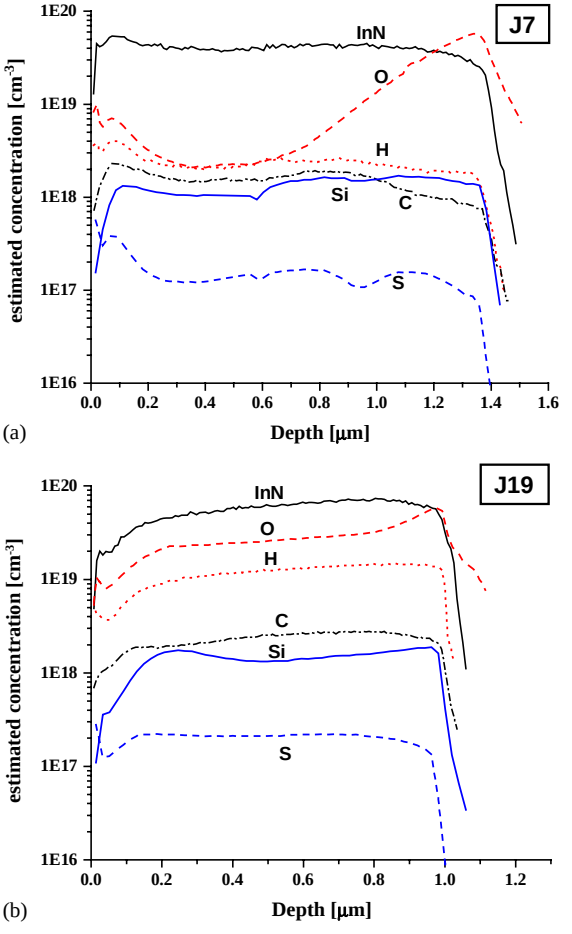

Fig. 5. (a) SIMS profiles of prominent contaminants in InN for sample J7. Oxygen and hydrogen profiles are calibrated, other profiles are in quasi-arbitrary units. (b) SIMS profiles of prominent contaminants in InN for sample J19. Oxygen and hydrogen profiles are calibrated, other profiles are in quasi-arbitrary units.

1 shows a comparison of the electronic properties, structural properties and calibrated chemical concentrations of various layers. Epilayers of set I show electron concentrations between 10^{20} and $5\times10^{20}\,cm^{-3}$ while epilayers of set II vary between $[n]=8\times10^{18}$ and $10^{20}\,cm^{-3}$. A reduction in oxygen concentration from set I to II coincides with a reduction in the measured free carrier concentration but no quantitative correlation could be established.

Photo-luminescence (PL) was measured at cryogenic temperatures (15 K) using a Ge detector

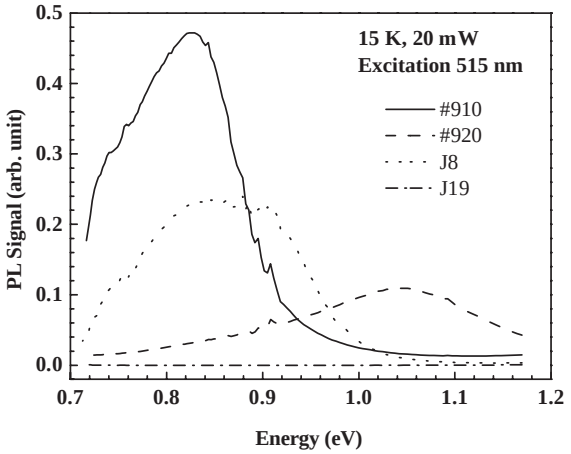

Fig. 6. PL spectra of selected InN epilayers. The signals are corrected for spectral sensitivity.

and an excitation wavelength of 515 nm. Fig. 6 shows the spectra of selected samples of both types. The data are corrected for spectral sensitivity. For a discussion of the Ge detector sensitivity for the case of InN PL see, e.g. Ref. [11]. Unexpectedly, epilayers with high oxygen concentrations and/or high-defect density exhibit PL while it is reduced by one order of magnitude in some epilayers of better crystalline quality. Sample J19 does not show any luminescence which is likely due to the incorporation of non-radiative defects, which may also be responsible for its electrical compensation: this sample has the lowest free electron concentration but lowest mobility, see Table 1.

The first series of InN epilayers grown at UC Berkeley (set I) shows a large variation of lattice constants. All samples are expected to contain more than $10^{20}\,cm^{-3}$ oxygen (first and last sample grown were measured by SIMS) due to insufficient vacuum conditions which were significantly improved between the different growth series and again after growth of J19. InN epilayers are known to be more sensitive to contamination than other group III—nitrides, which may be due to the necessity of low-temperature growth. All samples exhibit a similar surface topography as determined by AFM. The second set of samples has a smaller variation in lattice constants. Two samples (J5/J6) deviated significantly from the theoretical "a" lattice constant for strain-free InN [9]. The only noted difference in growth condition for those two samples is a lower temperature during substrate nitridation. A systematic study of the influence of the buffer layer growth conditions is currently under way. InN epilayers of set II have a very different surface topography than those of type I (see Fig. 3), but they are similar within the respective sample set and comparable to earlier published In-polar InN [11]. It is assumed that the variation of oxygen concentration from one set to the other is causing the topographical differences, because the known variations in growth temperature within one sample set or variations in the used buffer layers—for set I samples—did not have any noticable effect (except for an increase of the average grain size for the epilayers grown on MOVPE GaN buffers). It is possible that oxygen tends to segregate on specific crystallographic planes of InN, changing the growth rate on these planes and thus promoting growth of triangular-shaped features. More detailed TEM investigations which may support this suggestion are in progress. The high dislocation density found in the epilayers indicates that a lattice relaxation of the hetero-structural system occurred, which is expected for the deposited epilayer thicknesses. Nevertheless, several epilayers were found to be severely strained, especially those deposited on MOVPE GaN buffers. To date, the cause of the strain is still unknown.

It was assumed that the oxygen concentration [O] in InN epilayers may cause the high free electron concentration [n] as oxygen can act as a donor in InN. This investigation, however, shows that no consistent correlation between the oxygen concentration and the free electron concentration in InN exists. For set I samples a correlation $[O] \approx [n]$ exists. The second set of samples, however, consists of epilayers with significant higher oxygen than free electron concentration, approximately similar concentrations, and one sample with lower oxygen than the free electron concentration. The hydrogen concentration of the epilayers investigated here is at least one order of magnitude too small to account for the high free electron concentrations. Moreover, in the electrically compensated sample (J19) an increase of

hydrogen by a factor of four was observed which contradicts its role as dominant donor. Because of missing SIMS standards a quantitative analysis of most other chemical elements in InN was not possible. Therefore it is impossible at present to reach a conclusion on the role of silicon or sulphur as prospective donors in InN. However, we did not observe any significant changes in the SIMS profiles of those elements, so that changes in [n] cannot be correlated with any one of the investigated contaminants. Carbon as a prospective unintentional acceptor could also not be confirmed. As can be seen in Figs. 5a and b, the carbon profiles do not vary within the different epilayers. The role of native defects, V_N as a prospective donor and V_{In} as a possible compensating acceptor, will need to be investigated in the future.

The appearance of a broad PL signal at an energy around 0.8 eV, but changing in intensity, line shape and absolute energy position is a prominent feature in InN epilayers including materials with oxygen concentrations between more than $10^{20}\,cm^{-3}$ (reported here) and lower than $10^{17}\,cm^{-3}$ [14]. This investigation is focused on a comparatitive analysis of PL spectra obtained under the same conditions and corrected for spectral sensitivity. Because of the rapidly decreasing detector sensitivity in the energy range of these spectra an evaluation of energy peak positions or absolute intensities seems unfeasible. The appearance of weak PL peaks at higher energies (#920 in Fig. 6) is not correlated with the free electron or oxygen concentrations of the samples. In addition, those weak peaks are observed for similar epilayers in different energy ranges (compare #910 and #920 in Fig. 6). It is astonishing that the intensity of the 0.8 eV PL line obviously does not depend on the structural quality of the epilayer measured by the full width of half-maximum of a variety of X-ray diffraction reflexes. Symmetric and asymmetric reflexes, 0 0 2, 1 0 1 and 1 0 2 reflexes, were investigated and no correlation to the PL signal could be found. Within the first set of samples the epilayer with the lowest free electron concentration exhibited the strongest PL signal. However, this was also the highest intensity measured in comparison with the PL from the second set of epilayers so that a general correlation between the free electron concentration and the PL intensity also does not exist. The optical absorption of those samples follows the Moss–Burstein shift [6] and will be described elsewhere [8]. For set I epilayers there is also no correlation between the PL signal and the epilayer strain. This investigation is in progress for the second sample set.

4. Summary

MBE epilayer growth of InN was established with reproducible lattice constants. Those films show typical InN broad photo-luminescence around 0.8 eV and exhibit high free electron concentrations in the order of $10^{19}\,cm^{-3}$ with reasonably high electron mobility (up to $500\,cm^2/V\,s$). The residual contamination of those epilayers still has to be decreased. Epilayers deposited earlier (set I) contained more than one order of magnitude higher oxygen concentration, which is similar to the free electron concentration in those samples, respectively. The surface morphology between those two sample sets shows characteristic differences and seems to be related to the difference in oxygen content in the epilayers. The oxygen concentration of all epilayers does not alone explain the n-type conductivity of the respective films. Additional donors and/or acceptors or passivation elements in concentrations of the order of $10^{19}\,cm^{-3}$ must be present in several epilayers. Those dopants may be native defects. The large possible variation of the lattice constants, especially the c lattice constant, is unique for this group III—nitride compound but was only observed for selected samples of high oxygen concentration ($10^{20}\,cm^{-3}$). It can be explained by an anisotropic incorporation of contaminants along the basal planes of the InN crystal as the strain is typical for a uni-axial stress response.

Acknowledgements

This work was supported by the Director, Office of Science, Office of Basic Energy Sciences, Division of Materials Sciences and Engineering,

of the US Department of Energy under Contract No. DE-AC03-76SF00098.

References

[1] A.G. Bhuiyan, A. Hashimoto, A. Yamamoto, J. Appl. Phys. 94 (2003) 2779.
[2] M. Higashiwaki, T. Matsui, Jpn. J. Appl. Phys. 41 (2002) L540.
[3] T.L. Tansley, C.P. Foley, J. Appl. Phys. 59 (1986) 3241.
[4] B.E. Foutz, S.K. O'Leary, M.S. Shur, L.F. Eastman, J. Appl. Phys. 85 (1999) 7727.
[5] V.Yu. Davydov, A.A. Klochikhin, V.V. Emtsev, S.V. Ivanov, V.V. Vekshin, F. Bechstedt, J. Furthmuller, H. Harima, A.V. Mudryi, A. Hashimoto, A. Yamamoto, J. Aderhold, J. Graul, E. Haller, Phys. Stat. Sol. B 230 (2002) R4.
[6] J. Wu, W. Walukiewicz, K.M. Yu, J.W. Ager III, E.E. Haller, H. Lu, W.J. Schaff, Y. Saito, Y. Nanishi, Appl. Phys. Lett. 80 (2002) 3987.
[7] J. Wu, W. Walukiewicz, K.M. Yu, J.W. Ager III, E.E. Haller, H. Lu, W.J. Schaff, W.K. Metzger, S.R. Kurtz, J. Appl. Phys. 94 (2003) 6477.
[8] J. Wu, W. Walukiewicz, S.X. Li, R. Armitage, J.C. Ho, E.R. Weber, E.E. Haller, H. Lu, W.J. Schaff, A. Barcz, R. Jakiela, Appl. Phys. Lett. (2003), submitted for publication.
[9] A.F. Wright, J. Appl. Phys. 82 (1997) 2833.
[10] C. Kisielowski, In: Semiconductors and Semimetals, Vol. 57, 1999 p. 275–317 (chapter 7).
[11] K. Xu, A. Yoshikawa, Appl. Phys. Lett. 83 (2003) 251.
[12] V.S. Harutyunyan, A.P. Arivazyan, E.R. Weber, Y. Kim, Y. Park, S.G. Subramanya, J. Phys. D34 (2001) A35.
[13] W. Paszkowicz, R. Cerny, S. Krukowski, Powder Diffraction 18 (2003) 114.
[14] H. Lu, W.J. Schaff, L.F. Eastman, J. Wu, W. Walukiewicz, D.C. Look, R.J. Molnar, Mater. Rec. Soc. Symp. Proc. 743 (2003) L4.10.1.
[15] I. Vurgaftman, J.R. Meyer, J. Appl. Phys. 94 (2003) 3675.